Crack Blunting and Advancing Behaviors of Tough and Self-healing Polyampholyte Hydrogel

Feng Luo[1†], Tao Lin Sun[1†], Tasuku Nakajima[1], Takayuki Kurokawa[1], Yu Zhao[2], Abu Bin Ihsan[1], Hong Lei Guo[2], Xu Feng Li[2] and Jian Ping Gong[1*]

[1]*Faculty of Advanced Life Science, Hokkaido University, Sapporo 060-0810, Japan*

[2]*Graduate School of Life Science, Hokkaido University, Sapporo 060-0810, Japan*

*Corresponding author: gong@mail.sci.hokudai.ac.jp

[†]These authors contributed equally to this work.

Abstract:

Recently, we have reported that polyampholytes, synthesized from free radical copolymerization of anionic monomer and cationic monomer, form physical hydrogels of high toughness and self-healing. The random distribution of the opposite charges forms ionic bonds of a wide distribution of strength. The strong bonds serve as permanent crosslinks, imparting elasticity, whereas the weak bonds serves as reversible sacrificial bonds by breaking and re-forming to dissipate energy. In this work, we focus on the rupture behaviors of the polyampholyte physical hydrogel, P(NaSS-co-MPTC), copolymerized from sodium *p*-styrenesulfonate (NaSS) and 3-(methacryloylamino)propyl-trimethylammonium chloride (MPTC). Tensile test and pure shear test were performed at various stretch rates in the viscoelastic responses region of the material. Tensile test showed yielding, strain softening, and strain hardening, revealing the dually cross-linked feature of the gel. Pure shear test showed crack blunting at the notched tip, and a large yielding zone with butterfly-shaped birefringence pattern ahead of the crack tip. After blunting, crack advanced at steady-state velocity with a constant angle. The conditions for the occurrence of crack blunting and variables governing the crack advancing angle are discussed. We found that even for these highly stretchable samples, significant blunting only occurs when the tensile fracture stress σ_f is larger than modulus E by a factor of about two, in consistent with Hui's theoretical prediction for elastic materials. The crack advancing angle θ was found to be proportional to σ_y/E over a wide stretch rate range, where σ_y is the yielding stress. In addition, the fracture energy was correlated to small strain modulus by a power law in the viscoelastic response region. This systematic study will merit revealing the fracture mechanism of

tough viscoelastic materials including biological tissues and recently developed tough and highly stretchable hydrogels.

Keywords: hydrogel, soft material, polyampholyte, viscoelasticity, crack blunting, crack advancing, modulus, toughness

1. Introduction

Hydrogels are three-dimensional networks composed of crosslinked macromolecules and abundant water, belonged to soft & wet material. Based on some similarities to biological tissues, for example their soft and hydrated form, hydrogels have drawn great attention as synthetic equivalents for use in biological systems.[1-2] However, the scope of hydrogel applications is often severely limited by their mechanical weakness and brittleness. Recently, many hydrogels with excellent mechanical performance have been developed based on several different strategies.[3-8] Among them, the double network (DN) strategy has shown extra-ordinary effect on improving the toughness of hydrogels. DN hydrogels consist of interpenetrating polymer networks with contrasting mechanical properties. The first network is brittle and the second network is stretchable. The DN gels are as tough as rubbers and soft load-bearing bio-tissues. Double network hydrogels are tough because the internal fracture of the brittle network dissipates substantial amounts of energy under large deformation, while the elasticity of the second network allows it to return to its original configuration after deformation. Thus, the brittle network acts as a 'sacrificial bond' which breaks into small clusters to efficiently disperse the stress at the crack tip and increases the energy dissipate for crack propagation.[4] Since the rupture of the brittle network is due to breaking of the covalent bonds, which causes permanent damage, a DN gel shows permanent softening after large deformation, which will be a limitation in many practical applications. To address this problem, physically reversible bonds should be built in the hydrogel as a renewable 'sacrificial bond' to replace the irreversible covalent bonds. The hydrogen bond,[5] ionic bond,[6-7] Van der Waals interaction,[8] $\pi-\pi$ -interactions,[9] hydrophobic interactions,[10] are all potential candidates as renewable

'sacrificial bond'.[11-12] Studies along these lines have successfully produced tough double network hydrogels with self-recovery after internal rupture.[13-14]

The double network concept naturally suggests a more general strategy for developing tough hydrogels. That is, incorporating a mechanically fragile structure to toughen the material as a whole. This strategy means more freedom in the molecular design, not limited to double network but also applies to single network as long as it has sacrificial bond to dissipate energy and can retain original configurations of the material after large deformation, which has been realized using ionic bonds in hydrogels.[6] Based on this concept, recently, we have developed a novel class of tough and self-healing physical hydrogels from linear polyampholytes.[15] Polyampholyte hydrogels were synthesized using the one-step free radical copolymerization of equal-charge anionic monomer and cationic monomer. The randomly dispersed cationic and anionic repeat groups on the polymers form ionic bonds of a wide distribution of strength through inter-chain and intra-chain complexation. The strong bonds serve as crosslinkers, imparting elasticity, whereas the weak bonds serve as reversible sacrificial bonds by breaking and re-forming to dissipate energy. This class of hydrogels, belonging to supramolecular hydrogel and containing around 50 wt% water, exhibits many excellent mechanical properties, such as, tunable stiffness, high strength and toughness, damping, fatigue resistance, full self-recovery after large deformation, and high self-healing after cutting, along with biocompatibility.[15] The fracture toughness of polyampholyte hydrogels are ranked among the highest level of soft materials, either synthetic such as tough DN hydrogels,[16] highly stretchable double network gels,[13] and filled rubbers, or natural bio-tissues , such as cartilages.[17]

Studying of the fracture behavior of the polyampholyte hydrogels should help us to clarify the toughening mechanism of the viscoelastic and highly stretchable materials. In this study, we systematically studied the fracture behaviors of a polyampholyte system poly(NaSS-co-MPTC) copolymerized from anionic monomer sodium *p*-styrenesulfonate (NaSS) and cationic monomer 3-(methacryloylamino)propyl-trimethylammonium chloride (MPTC). According to our previous report, this system has a water content of 52 wt%, a softening temperature at 48.2°C.[15] Furthermore, around room temperature (24.1°C), the dynamic shear modulus G' follows a power law with the frequency f as $G' \sim f^{0.32}$ in the frequency range (10^{-3}-10^{0} Hz), and the loss factor tanδ has a broad peak around 0.05 Hz, which gives a characteristic relaxation time $\tau_w = 1/(0.05 \times 2\pi) \approx 3$s.[15] This time is considered as the average bond exchange time of the weak bonds.

In this paper, we first present the tensile behaviors at various stretch rates, in the range below and close to the inverse of the weak bonds relaxation time τ_w. Strain softening at intermediate deformation and strain-hardening at large deformation were clearly observed in the Mooney plot, which demonstrates the dually cross-linked feature of the gel in the observation time scale. Interestingly, we also observed a master curve of reduced stress vs time at various stretch rates, similar to that reported by Mayumi et al.[18] Then, we adopted a classical pure shear test to observe the crack morphology change and to measure the crack advancing resistance at different stretch rates. Fracture energy exhibits notable dependence on the stretch rate. *In-situ* observation of detailed fracture behavior of this hydrogel undergoing different stretch rates was performed by using a pair of polarized optical films. Blunting of the crack tip and large yielding zone with the butterfly-shaped birefringence pattern were observed around the crack tip. Finally, we

discuss the conditions for the occurrence of crack blunting and variables governing the crack advancing angle. Significant blunting was found to occur when the tensile fracture stress σ_f is larger than modulus E by a factor of about two, in consistent with Hui's theoretical prediction for elastic materials.[19] The quantity $\theta E/\sigma_y$ was found to be independent of the stretch rate over a wide range, indicating that θ is proportional to σ_y/E, where σ_y is the yielding stress. In addition, the small strain modulus and the fracture energy are correlated by a power law in the viscoelastic response region where blunting occurs. This systematic study will merit revealing the fracture mechanism of tough viscoelastic materials including biological tissues and recently developed tough and highly stretchable hydrogels.[13-14, 18]

2. Experiment section

2.1 Materials

Commercially available anionic monomer, sodium *p*-styrenesulfonate (NaSS); cationic monomer, 3-(methacryloylamino)propyl-trimethylammonium chloride (MPTC); UV initiator, α-ketoglutaric acid; and NaCl are all purchased from Wako Pure Chemical Industries, Ltd. and used as received. Millipore de-ionized water is used in all of the experiments.

2.2 *Synthesis of polyampholyte physical hydrogels*

Polyampholyte physical hydrogels are synthesized using the one-step free radical copolymerization of the anionic monomer and the cationic monomer, according to the method described in our previous reports.[15, 20] Briefly, A mixed aqueous solution of total monomer concentration C_m (=[NaSS] + [MPTC]) of 2.0 M with optimized molar fraction

of the anionic monomer f (=[NaSS]/C_m) at 0.525, 0.1mol% UV initiator (in relative to C_m), and 0.5 M NaCl (used to control the ion strength) was injected into a reaction cell (10 cm ×10 cm) consisting of a pair of glass plates with a 1 mm silicone spacer. The polymerization was carried out in argon atmosphere in which the oxygen concentration was less than 0.1 ppm by irradiating with 365 nm UV light (UVPlampXX-15BLB, light intensity ~ 4mW/cm^2) from both sides for 8 hours. After polymerization, the hydrogels were immersed in a large amount of water for 1 week to reach equilibrium, and the water was changed every day. During this process, the hydrogels shrank due to formation of ion bonds between the opposite charges on the polymer and their mobile counter ions were dialyzed from the hydrogels. After reaching the equilibrium state in water, the hydrogel thickness changed from 1mm in the as-prepared state to 0.85 mm in water. The water content of the hydrogel at the equilibrium was 52 wt%.

2.3 Characterization of hydrogels

Tensile test. The tensile test was carried out on dumbbell-shaped samples with the standard JIS-K6251-7 size (35 mm (L) × 2 mm (w) × 0.85 mm (d)) using a commercial tensile tester (Tensilon RTC-1310A, Orientec Co.). The initial distance L_0 between the two clamps of the tester was 12 mm and the tensile deformation was performed at a series stretch velocities v from 1 to 500 mm/min., which gives the stretch rate $\dot{\varepsilon} = v/L_0$ from 0.0014 to 0.7 s^{-1}. This stretch rate range corresponds to $\dot{\varepsilon}\tau_w$=0.004~2.1. The nominal stress σ was estimated from the stretch force divided by the cross-section area of the undeformed sample. The strain ε was estimated from the clamp displacement divided by L_0.The Young's modulus E was estimated as the slope of the stress-strain curve within a

strain range of ε=0.03-0.1. The yield stress, $\sigma_{y,}$ was obtained at which the tangent modulus $d\sigma/d\varepsilon$ changes at the greatest rate with respect to increasing strain. The values of all the mechanical properties were calculated as averages for at least three specimens. All of the measurements were performed in a water bath made from a transparent box at about 25 °C except specified.

Pure shear test. A pure shear test was performed using the above tensile tester at a series stretch velocities from 1 to 500 mm/min, following the method established in references.[13, 21] Two different samples, single-edge notched (pre-crack) and unnotched, were used to measure the fracture energy Γ. The samples were cut into a rectangular shape with a width of 20 mm and length 40 mm (a_0). An initial notch of 10 mm (a) in length was cut using a razor blade. The test piece was clamped on two sides, and the distance between the two clamps was fixed at 8 mm (L_0). This gives stretch rate $\dot{\varepsilon} = v/L_0$ from 0.002 to1.04 s^{-1}, higher than that of the tensile test by a factor of 3/2 at the same tensile velocity. The force-displacement curves of the samples were recorded, and the fracture energy Γ was calculated from

$$\Gamma = U(L_{c1})/(a_0 \times b_0), \qquad (1)$$

where b_0 was the sample thickness (0.85 mm), $U(L_{c1})$ is the work done by the applied force to the unnotched sample at the critical stretching displacement L_{c1} of the moving clamp, where L_{c1} is the displacement at which the crack growth initiates in the notched sample. The onset of the crack growth was determined using the movie image recorded by a video camera. The crack growth velocities as a function of displacement at various

stretch velocities were obtained by carefully analysing the movies during crack growth. All of the experiments were also carried out in the transparent water bath at about 25 °C.

In order to tune the strength of the ionic bonds, we also changed the temperatures (5, 10, 15°C) and the ionic strength of the bath solution (0.01, 0.05, 0.154, 0.3, 0.5 M). For the latter test, the hydrogels are equilibrated in these solutions for one week, and then the test was performed at a fixed stretch rate of 0.2 s^{-1}. The volume change of the sample in these two sets of experiment was almost negligible.

Besides, two control tests for samples at high stiffness and brittleness state were performed. One was using a sample quenched at low temperature (5^{o}C) and tested at fast stretch velocity 500 mm/min (stretch rate 1.04 s^{-1}). The other was using a partially dehydrated sample with water content 26wt% and tested at stretch rate 0.2 s^{-1} in 25°C. For these samples, the observation time was selected to be much shorter than the bond exchange time.

In-situ observation of deformation and fracture. To observe the stress distribution during deformation and fracture, a home-made circular polarizing optical system was combined with the tensile tester both in tensile test and pure shear test (**Figure 1**). Two pieces of circular polarizer films were fixed, respectively, on the front and back surfaces of the transparent water bath box. A white lamp and a video camera were installed in front side and back side of the box, respectively. The video camera recorded the shape and isochromatic images of the samples during test. The optical retardation change of the samples during the tensile test was estimated by comparing the birefringence colors with

a Michel-Levy chart.[22-23] This simple method tells, roughly, the stress distribution of the samples during deformation.

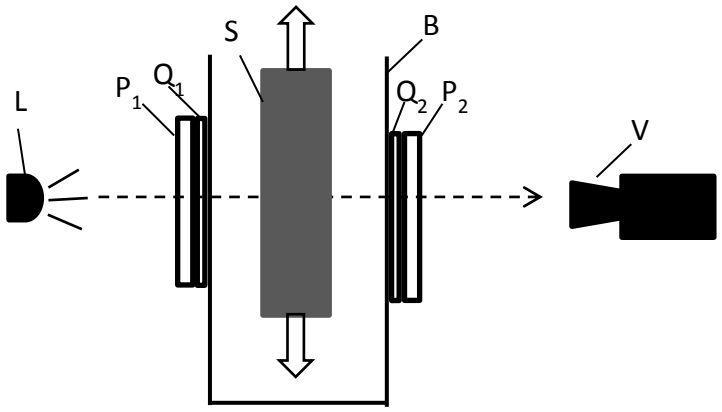

L: lamp, P_1, P_2 : polarizer, Q_1,Q_2: quarter wave retarder plate, P+Q: circular polarized film, S: sample, B: water bath, V: video camera . The sample was stretching in the direction shown by arrows.

Figure 1. Schematic diagram of in-situ optical observation in tensile test and pure shear test.

3. Results

3.1 Uniaxial tensile behaviors

To ascertain the nonlinear and viscoelastic behaviors of the polyampholyte hydrogels at large deformation, we performed uniaxial stretching experiments at various stretch rates, and the tensile stress-strain curves (nominal stress σ vs nominal strain ε) are plotted in **Figure 2a**. Apparently, the mechanical properties are strongly influenced by the stretch rates. Clear yielding phenomenon is observed around a strain ε=0.5 and the yield stress increases from 0.06 MPa to 0.68 MPa, as the stretch rate increasing from 0.0014 to 0.7 s^{-1}.

The fracture stress also increases with the stretch rate from 0.75 MPa to 3.44 MPa, while the fracture strain decreases with the stretch rate. The Young's modulus E of samples notably increases about 13 times with the 500 times increase in the strain rate from 0.24 MPa at 0.0014 s^{-1} to 3.16 MPa at 0.7 s^{-1}. The E follows a power-law relation with the stretch rate, $E \sim \dot{\varepsilon}^{0.41}$, as shown in **Figure 2b**. This power law is slightly stronger than but close to that observed from the dynamic measurement ($G' \sim f^{0.32}$) in the same dynamic range.[15]

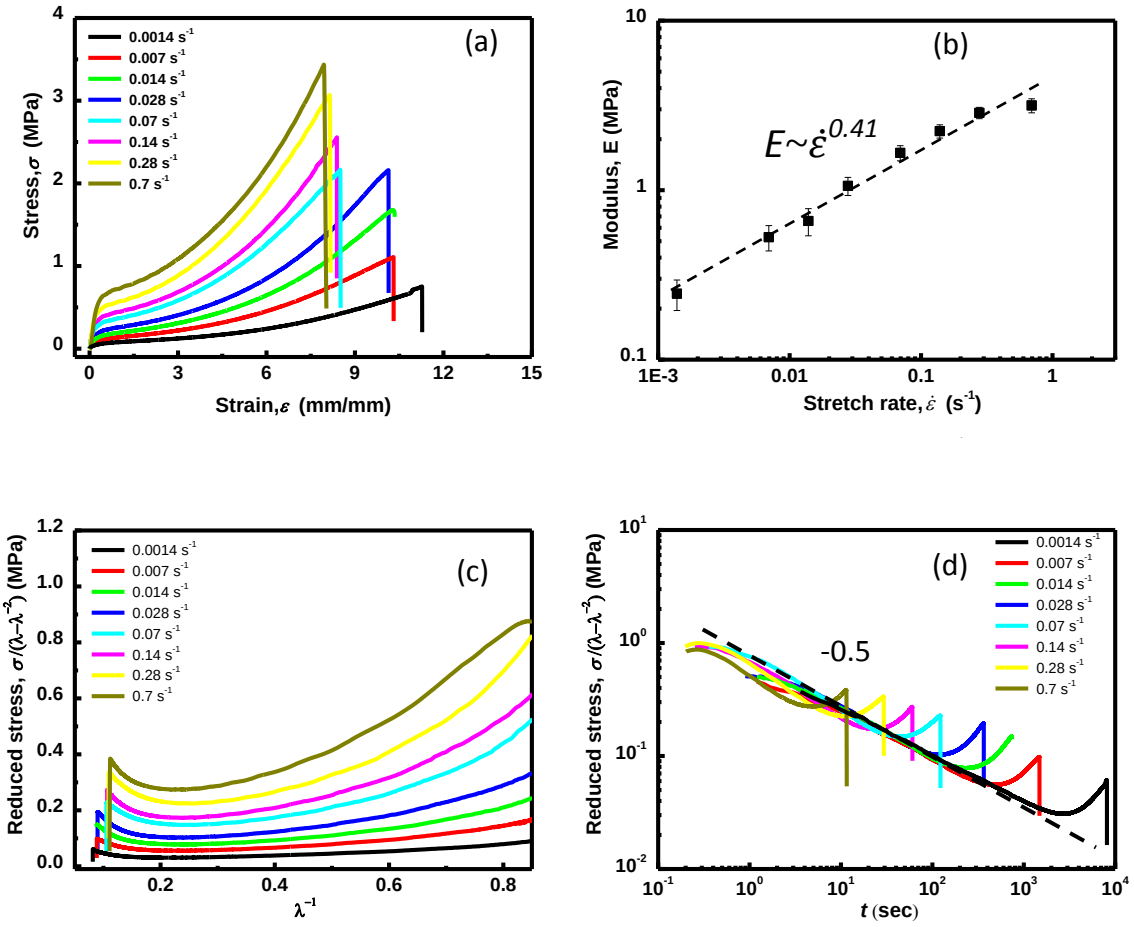

Figure 2. (a) Tensile stress-strain curves for the polyampholyte hydrogels at various stretch rates; (b) The modulus of samples at various stretch rates, it follows a power-law relation to stretch rate $E\sim\dot{\varepsilon}^{0.41}$; (c) Reduced stress $\sigma^*=\sigma/(\lambda-\lambda^{-2})$ as a function of λ^{-1} for the hydrogels at various stretch rates; (d) Time dependence of the reduced stress σ^* for the hydrogels at various stretch rates, the slope of dash line is -0.5. Values in (a), (c), and (d) are stretch rate. In (c) and (d), the data at very short time, which may contain an inaccuracy coming from the apparatus due to the acceleration of the traction, are not shown.

In the previous report, it has been revealed that the randomness of the charge distribution of the polyampholyte makes ionic bonds of a wide distribution of strength. The strong ionic bonds serve as permanent crosslinks, imparting elasticity, whereas the weak ionic bonds serve as reversible sacrificial bonds to dissipate energy.[15] This picture is further confirmed in the present work by the features observed in the Mooney plot of the stress-strain curves, where the reduced stress $\sigma^* = \sigma/(\lambda - \lambda^{-2})$ is plotted as a function of $1/\lambda$ (**Figure 2c**). Here σ is the nominal stress and $\lambda = \varepsilon + 1$ is the stretch ratio. As shown in **Figure 2c**, at large $1/\lambda$, the σ^* - $1/\lambda$ plot has a positive slope, indicating the occurrence of strain softening. The strain softening that becomes more prominent at high stretch rate, is the clear evidence of weak bonds breaking. On the other hand, the σ^* - $1/\lambda$ plot has a negative slope at small $1/\lambda$, indicating the occurrence of strain hardening. This strain hardening is the evidence of the existence of strong bonds that do not break at the observation time scale and give finite extensibility of polymer chains. As the maximum extensibility and strain-hardening are stretch rate dependent, the strong bonds also have relaxation distribution in the observation time scale.

According to a recent report by Mayumi et al., the effects of strain and time can be separated for a polyvinyl alcohol (PVA) hydrogel with dual cross-linking, one is permanent chemical crosslinking and the other is reversible physical crosslinking.[18] Following Mayumi et al's method by plotting the reduced stress σ^* against the time of stretching t, we also find the similar deformation-time separable behavior in the present system. As shown in **Figure 2d**, all the curves overlap except for the strain hardening regimes where the reduced stress increases rapidly with time, so that a master curve of reduced stress vs time is exhibited, with a slope close to -0.5. As the physical cross-links

of polyampholyte hydrogels rupture during deformation, $\sigma^*(t)$ decreases with t. The decrease of σ^* is dominated only by time t and independent of strain, which indicates that strain and strain rate have no influence on the breakage rate of the weak bonds of the hydrogels. These behaviors are similar to the dually cross-linked PVA hydrogel.

To better understand the deformation behavior during tensile test, quantitative analysis of the birefringence colors of the samples by deformation is accomplished. The in-situ recording video and some typical photographs of the hydrogel stretched at $\dot{\varepsilon} = 0.14\ s^{-1}$ are presented in **Movie S1** and **Figure S1a** of supporting information (SI), respectively. The samples show uniform deformation with the increasing of strain ε, and no necking occurs. The birefringence color, reflecting optical retardation, shifts with the increase of stretching and well complies with the Michel-Levy chart from left to right. The optical retardation (r) determined from the Michel-Levy chart is related to the birefringence (Δn) by $\Delta n = r/(b_0/\sqrt{\lambda})$. Here, b_o is the sample thickness at undeformed state, $\lambda=\varepsilon+1$ the stretch ratio, and we assume the hydrogel is incompressible. The Δn as a function of strain ε are plotted in **Figure S1b**. As a result of strong molecular interaction in the polyampholyte gels, the birefringence almost linearly increased with the increase of strain ε, even at very small strain. This is quite different from common highly stretchable hydrogels that the birefringence only starts to appear at relatively large strain.[24] The true stress σ_t against the strain ε is also shown in **Figure S1b**, where σ_t is obtained from the nominal stress σ by $\sigma_t = \lambda\sigma$. The true stress showed a slight strain weakening above ε=0.5. As a result, the birefringence-true stress plot shows two linear regions with a reflection point at birefringence Δn=0.003, corresponding to strain ε =1.5 (**Figure S1c**).

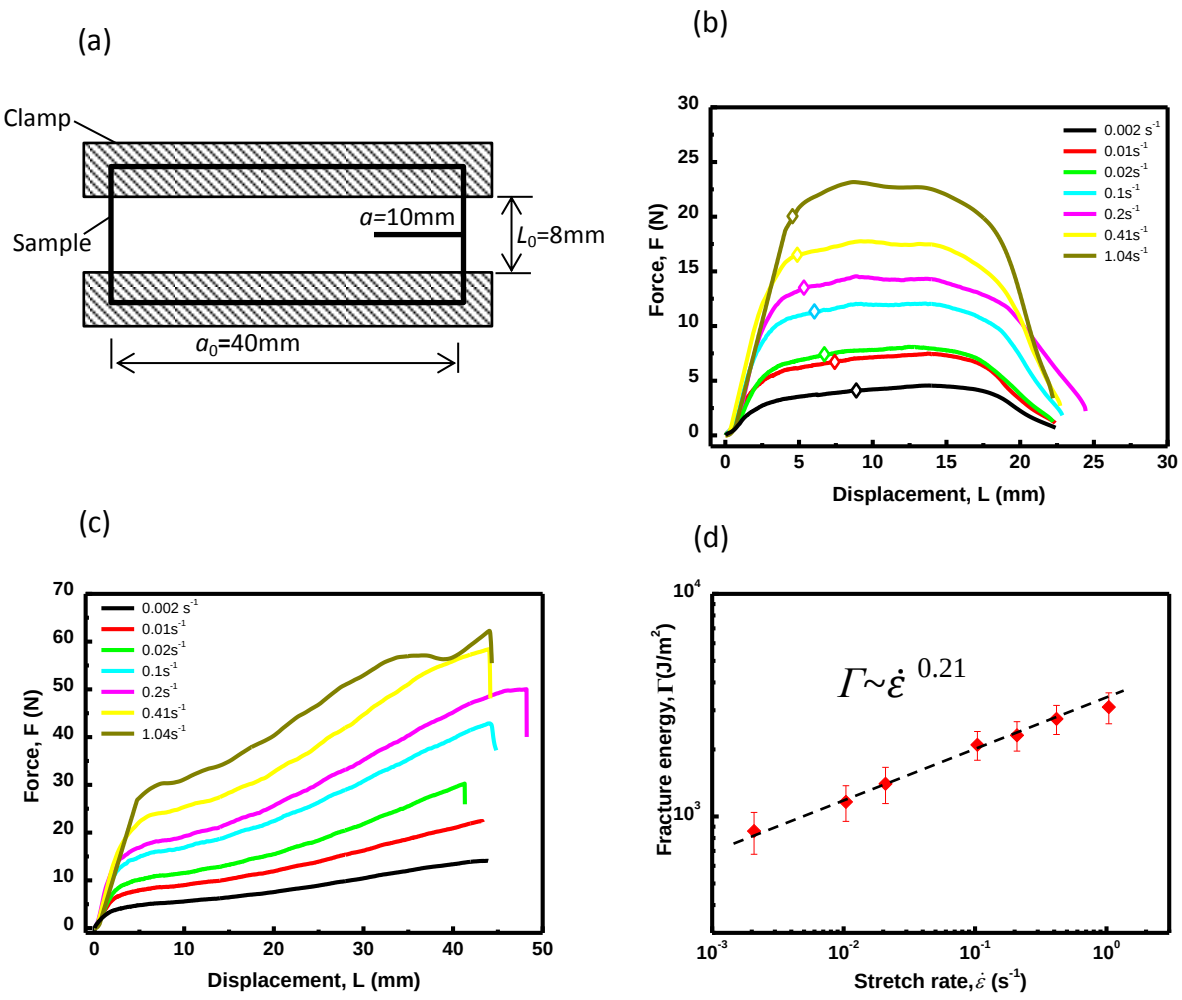

Figure 3. The fracture behaviors of the polyampholyte hydrogels. (a) Geometry of notched sample for pure shear test; (b) Force-displacement curves for notched samples at various stretch rates, the critical points of crack advancing is marked on each curve by the diamond square; (c) Force-displacement curves for unnotched samples at various stretch rates; (d) Fracture energy vs stretch rate, the fracture energy follows a power-law $\Gamma \sim \dot{\varepsilon}^{0.21}$.

3.2 Pure shear behaviors

To clearly evaluate the fracture toughness and fracture behaviors of hydrogels, the classical pure shear test for measuring fracture energy of soft materials is performed.[21, 25] The geometry of notched sample for pure shear test, and force-displacement curves for both notched and un-notched samples at various stretch rates are shown in **Figure 3a-c**. The yielding stress of unnotched samples exhibits strong stretch rate dependence, in agreement with the behaviour observed in tensile test (**Figure 2a**), while the elongation at breaking of samples is almost insensitive to the stretch rate, which is quite different from the tensile test. Thus, the geometry of the measurement substantially influences the mechanical behaviours at large deformation. The fracture energy Γ calculated by Eq. 1 shows a power-law relation with the stretch rate as $\Gamma \sim \dot{\varepsilon}^{0.21}$ **(Figure 3d)**. The higher stretch rate results in higher fracture energy dissipation of samples. With the change of the stretch rate from 0.002 to 1.04 s^{-1}, the fracture energy increases from 860 to 3100 J/m^2. This fracture energy Γ contains both the energy for mechanical dissipation in regions around the crack due to viscoelasticity and the intrinsic fracture energy required to break polymer chains or the chain association lying across the crack plane.

Unique crack shape evolution and crack advance were observed during the pure shear test. As typical example, the force-displacement curve and isochromatic images of a notched hydrogel testing at strain rate of 0.02 s^{-1} were shown in **Figure 4a** and **4b**, respectively. The movie is available in SI (**Movie S2)**. From starting point of stretch (A) to yielding point (C), the stress gradually concentrated at the notched tip, as revealed by the notable isochromatic images, and the crack did not advance. The notched tip showed an obvious crack blunting behavior at B. The blunting developed with the further increase of the

strain, and the stress around the semi-circular shaped crack remained the same level, as revealed by the isochromatic images from C to E. With the further increase of the displacement, a small triangle was observed in the middle of the blunting circular arc at F (schematic image of **Figure 4c**). In accompanying with this shape change, the stress at the notched tip increased sharply, as observed by the color of the isochromatic image. From F, the crack started to advance with the increase of the displacement, accompanying a strong stress concentration pattern at the tip of crack (F). Beyond F, the crack advanced in steady-state with a constant triangle shape. After H, the free edge effect came into play and the crack growth was accelerated, as shown by the merging of stress concentration pattern at the crack tip with that of free edge. **Figure 4c** shows illustrations of crack shape at various stages.

The angle θ at the crack tip after forming triangle was analyzed. As shown in **Figure 4a**, when the crack grew at a steady velocity in phase with the stretch velocity (F to H), θ almost kept a constant value at 115°. The isochromatic patterns indicate that the stress at the crack tip was almost constant. After I, the un-notched edge became very close to the crack tip. As a result, the angle of crack tip decreased sharply. In sequent, a secondary angle was formed (J) and the angle increased rapidly in accompany with the rapid decrease in the stress (K) until sample fracture.

(a)

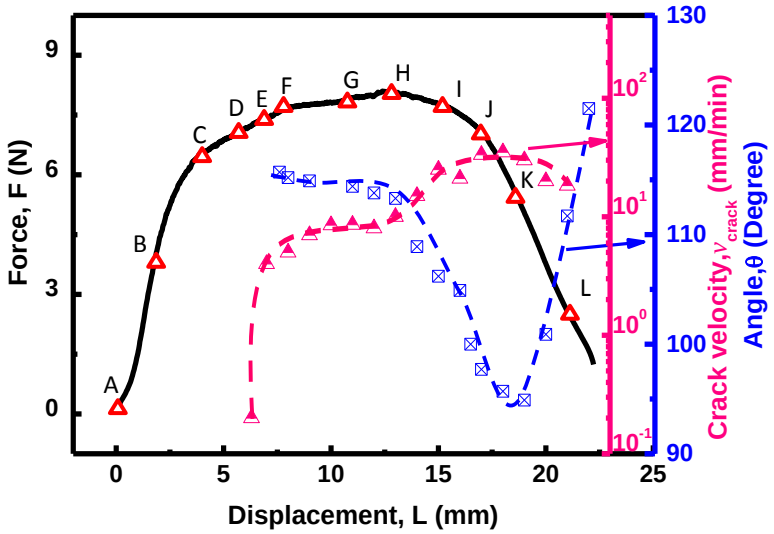
Force, F (N)
Displacement, L (mm)
Crack velocity, v_{crack} (mm/min)
Angle, θ (Degree)
A
B
C
D
E
F
G
H
I
J
K
L

(b)

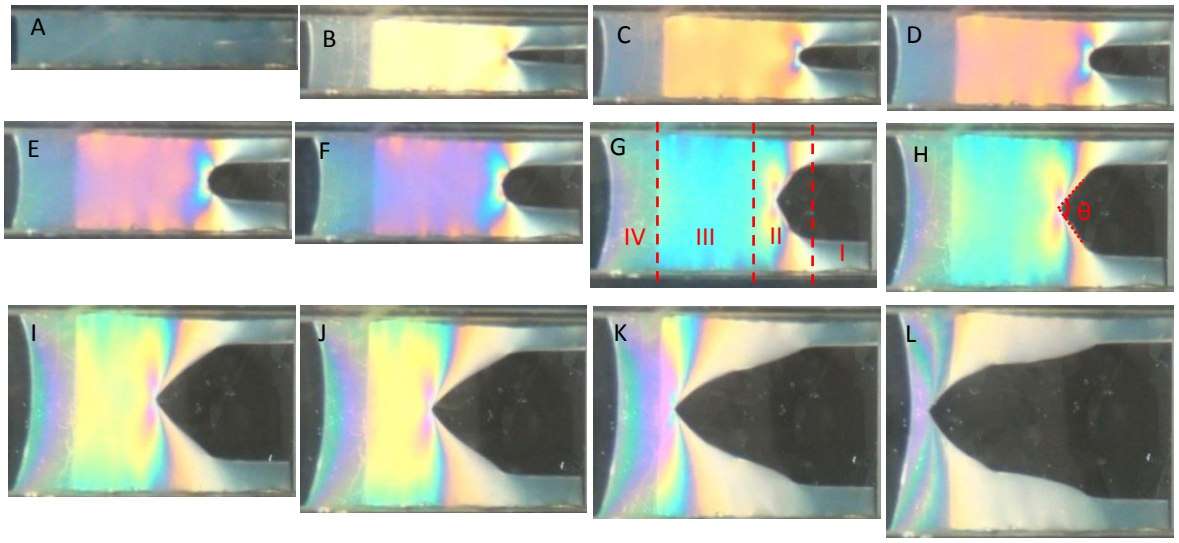
A
B
C
D
E
F
G
IV
III
II
I
H
θ
I
J
K
L

(c)

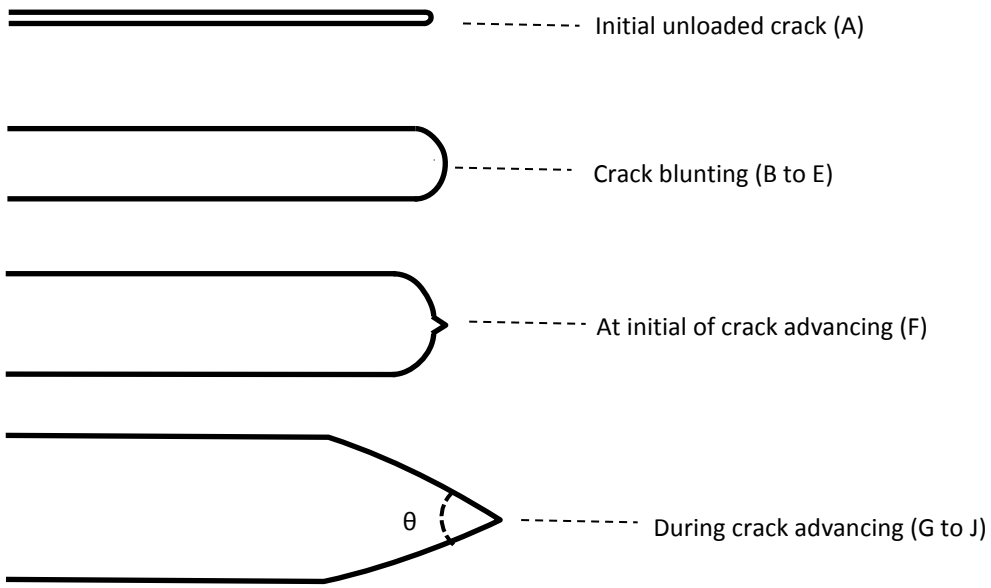

Figure 4. (a) Typical force curve at various displacements for a notched hydrogel sample testing at $\dot{\varepsilon}$ =0.02 s^{-1}. The angle θ of crack tip and the crack growth velocity obtained from the images in (b) are also shown. (b) Typical sample images (location A to L marked in Figure a) of pure shear test, image B is the start of blunting, image F is the start of crack growth, image G shows four different strain regions of notched hydrogel sample during test. (c) Schematic diagrams of the development of crack tip.

The crack advance velocity v_{crack} as a function of displacement is also shown in **Figure 4a**. When the crack started to growth at F, the crack velocity increased with the displacement and then reached at a constant value a little beyond F. After H, the crack growth is an accelerated process, influenced by the un-notched free edge. These behaviors are well in agreement with the changes in the angle of the crack and the stress distribution around the crack.

According to the stress distribution during test, the sample in steady-state crack growth can be divided into four different strain regions as shown in **Figure 4b-Image G**. Region I is undeformed region in which the stress can be ignored because of the presence of crack. Region II around the crack tip has a complicated stress field. Ordinal interference color from far to near around the crack tip and a butterfly-shaped stress concentration zone perpendicular to the crack tip can be observed. The latter indicates that this region suffers a shearing yielding under plane strain and plane stress.[26] This shear yielding of material absorbs a lot of energy and retards the propagation of crack. Therefore, this kind of material shows high toughness. Such kind of butterfly-shaped pattern usual can be found in tough plastic or polymer elastomers but few found in hydrogels.[19, 27] Region III that is far from the crack tip is the pure shear zone with uniform interference color. Region IV is force free edge zone that slightly deviates from the pure shear state.

3.3 Stretch velocity effect on fracture behavior

Considering the strong viscoelastic nature of the polyampholyte hydrogels, we further analysed the effect of stretch velocity on the crack blunting and growth process of the gel.

The crack growth velocity v_{crack} as a function of displacement at various stretch velocities v is plotted in **Figure 5a**. Three critical stretch ratios for initiation of crack growth λ_{c1}, for starting of the steady-state crack growth λ_{c2}, and for starting of the accelerated crack growth λ_{c3} at various stretch rates $\dot{\varepsilon}$ are observed, and their stretch rate dependences are shown in **Figure 5b**. These critical stretch ratios are defined as $\lambda_c=L_c/L_0+1$, where L_c is the corresponding critical displacement. The crack growth velocity v_{crack} showed three stages regardless of the wide stretch velocity range investigated. At the initial stage above λ_{c1}, the crack velocity increased with the displacement. Above λ_{c2}, the second stage started and the crack grew roughly at a constant velocity. The third stage above λ_{c3} was an accelerated crack propagation at the later part of crack growth, influenced by the un-notched free edge. The stretch ratio λ_{c1} for the transformation from crack blunting to growth shifted to small value with increasing stretch rate. Similar stretch rate effect was also observed for the onset of the steady-state crack growth, which also showed a shift of λ_{c2} to small value with increasing stretch rate. On the other hand, the onset of the third stage is independent on the stretch rate and all occurred at $\lambda_{c3}=2.7$. The latter result confirms that the third stage is due to the influence of the unnotched edge, in agreement with the result in **Figure 4b**. The crack growth velocity at the second steady-state stage was almost equal to the corresponding stretch velocity (**Figure 5c**). It was confirmed that when the stretching at this stage was stopped, the crack growth also stopped instantly. This is different to brittle hydrogels that the crack will spontaneously propagate above a critical strain.[25] While at the third stage, the crack propagation also stopped but with delay when the stretching was stopped to increase.

(a)

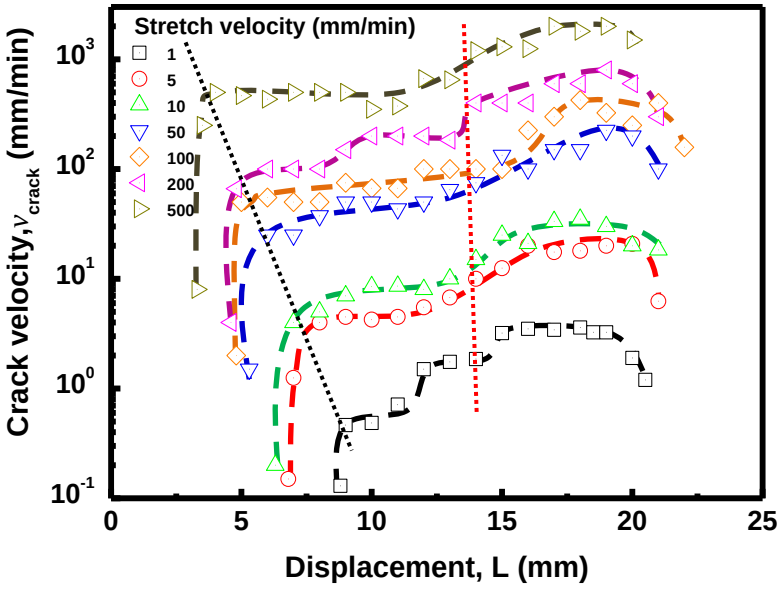
Stretch velocity (mm/min)
1
5
10
50
100
200
500
Crack velocity, v_{crack} (mm/min)
10^3
10^2
10^1
10^0
10^{-1}
0
5
10
15
20
25
Displacement, L (mm)

(b)

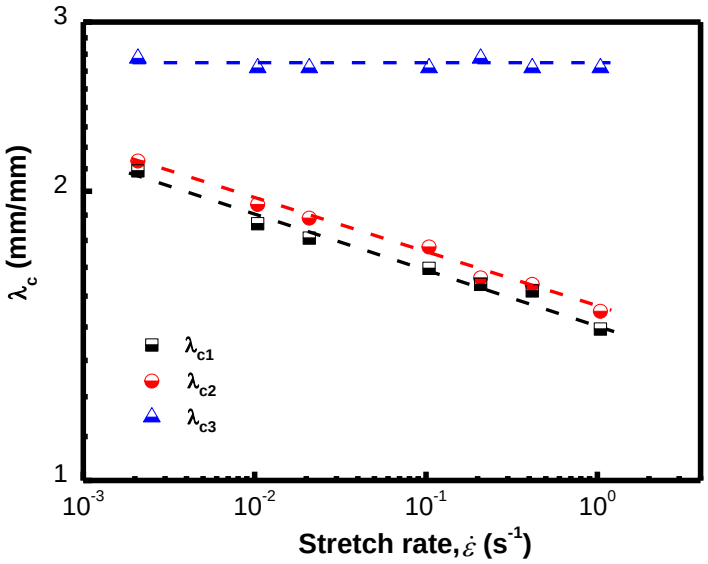
3
2
1
λ_c (mm/mm)
λ_{c1}
λ_{c2}
λ_{c3}
10^{-3}
10^{-2}
10^{-1}
10^0
Stretch rate, $\dot{\varepsilon}$ (s^{-1})

(c)

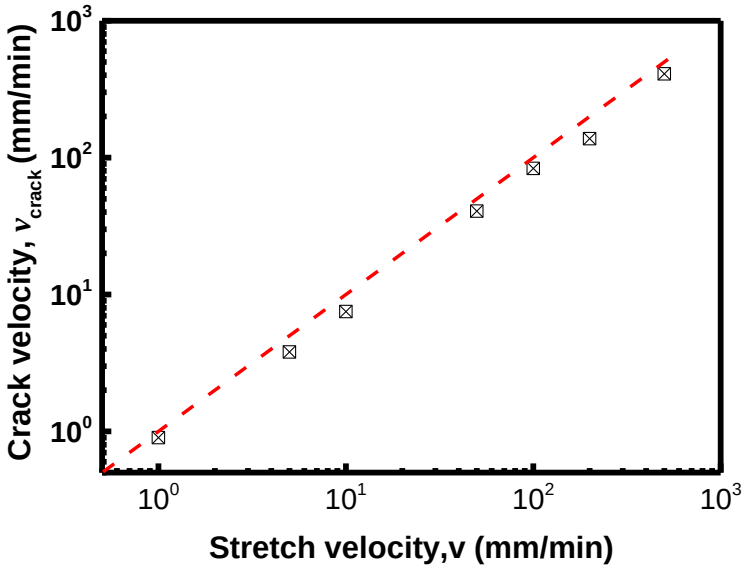

Figure 5 (a) The crack velocity v_{crack} vs displacement at various stretch velocities; the black dotted line denotes the onset of steady-state crack growth and the red dotted line denotes the onset of accelerated crack propagation. (b) critical stretch ratios for starting of crack growth λ_{c1}, for starting of the steady-state crack growth λ_{c2}, and for starting of the accelerated crack growth λ_{c3} at various stretch rates; (c) average velocity of steady state crack growth velocity v_{crack} at various stretch velocities v, the red dash line represents crack growth velocity = stretch velocity.

In the steady state crack growth stage, the shape of the crack tip changes with the stretch velocity. **Figure 6a** shows the typical photographs of crack propagation of samples at various stretch rate at strain ε=1.5 (displacement L=12 mm). At this strain, all the samples are in the steady-state crack growth, exhibiting a triangle-shaped crack with a butterfly-shaped stress concentration zone perpendicular to the crack tip. Particularly, the angle of the crack and birefringence color both in butterfly-shaped zone and in pure shear zone changed with stretch rate. The angle of crack, the retardation (birefringence color) at butterfly-shaped zone, and the retardation in pure shear zone are plotted as a function of stretch rate in **Figure 6b**. The angle of the crack decreased from 122° to 95° with increasing stretch rate from 0.002 to 1.04 s^{-1}. Meanwhile, the retardation for butterfly-shaped zone shifted from 700 nm (bright blue) to 1560 nm (light pink). For the pure shear zone, birefringence color shifted from 400 nm (orange) to 1250 nm (cyan). Since the retardation is directly proportional to true stress, the results indicate that the stress required for the crack growth increases with the stretch rate.

(a)

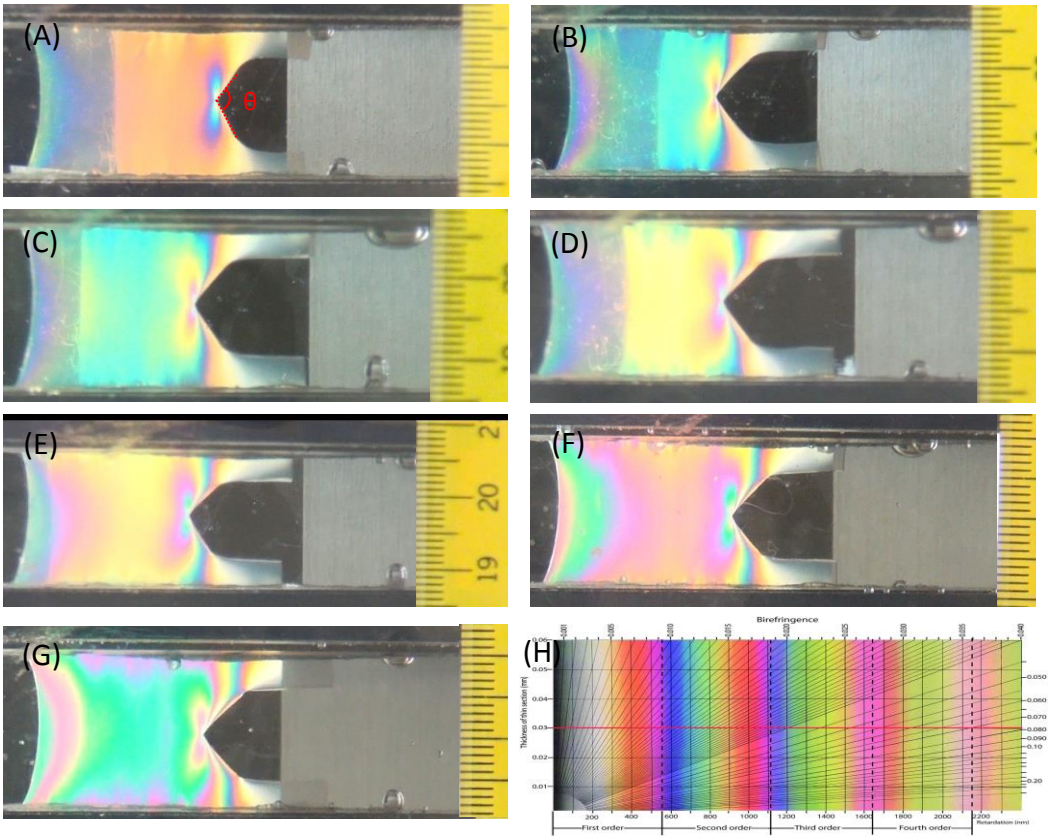
(A)
θ
(B)
(C)
(D)
(E)
(F)
(G)
(H)
Birefringence
First order
Second order
Third order
Fourth order

(b)

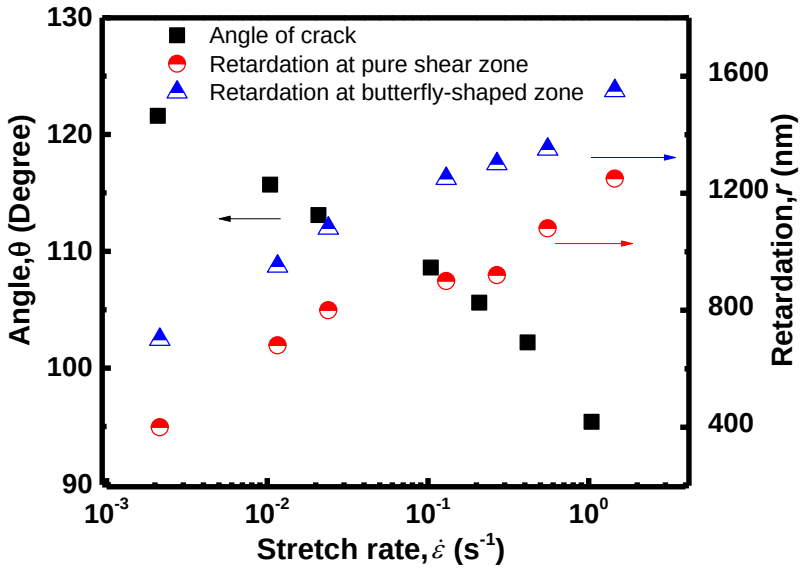
Angle of crack
Retardation at pure shear zone
Retardation at butterfly-shaped zone
Angle,θ (Degree)
Retardation,r (nm)
Stretch rate, $\dot{\varepsilon}$ (s^{-1})
130
120
110
100
90
1600
1200
800
400
10^{-3}
10^{-2}
10^{-1}
10^{0}

Figure 6. Pure shear test results for samples in the steady-state crack growth stage undergoing various stretch rates at strain ε=1.5. (a) Photographs of samples, each scale in right side of pictures is 1 mm; (A) $\dot{\varepsilon}$ =0.002 s^{-1} (B) $\dot{\varepsilon}$ =0.01 s^{-1} (C) $\dot{\varepsilon}$ =0.02 s^{-1} (D) $\dot{\varepsilon}$ =0.1 s^{-1} (E) $\dot{\varepsilon}$ =0.2 s^{-1} (F) $\dot{\varepsilon}$ =0.4 s^{-1} (G) $\dot{\varepsilon}$ =1.04 s^{-1} (H) a Michel-Levy chart.

(b) The angle θ of crack and the retardation at both butterfly-shaped zone and pure shear zone of hydrogel samples undergoing various stretch rates at strain ε=1.5.

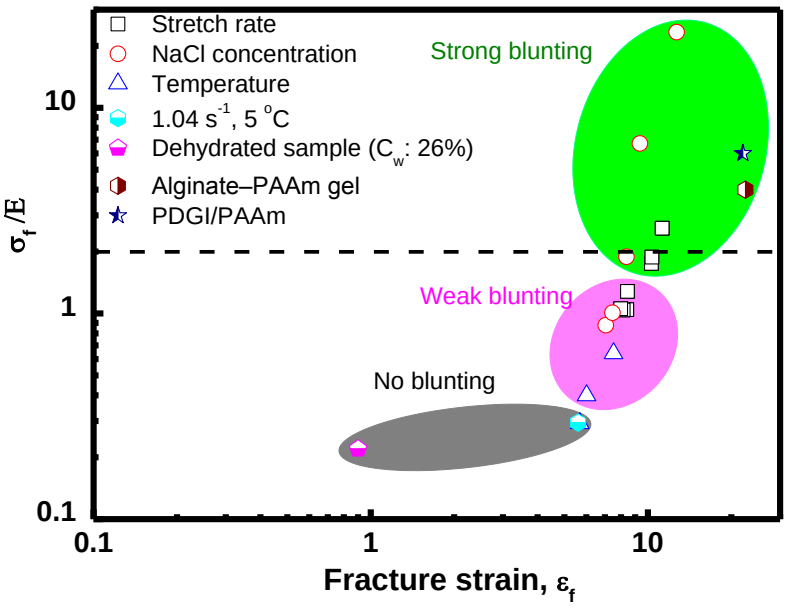

Figure 7. Correlation between the crack blunting behaviors and the tensile behaviors of the polyampholyte hydrogel measured at various conditions. Here, E, σ_f, and ε_f are Young's modulus, fracture stress, and fracture strain of the sample in tensile test, respectively. The dotted line indicates the board for the blunting of elastic material, σ_f/E=2 theoretically obtained by Hui et al (reference19). Data of Alginate-PAAm gel and PDGI/PAAm gel are from references 13 and 14, respectively.

4. Discussion

Blunting condition. The blunting of a highly stretchable soft material with non-linear mechanical behaviour is not well understood yet. Some studies has revealed that the crack blunting of pre-crack samples occurs when the cohesive stress exceeds the elastic modulus.[28-29] Blunting of a linear elastic material has been theoretically studied by Hui et al.[19] They showed that blunting has essentially to do with large deformation, and occurs when the cohesive stress σ_o exceeds the elastic modulus E.[19] This is because an increase in remote loading results in a tendency for crack tip stress to increase. However, this increase in crack tip stress is mitigated by an increasingly blunted shape. A comparison of the two tendencies yields the condition for blunting. Assuming that the crack deforms in a series of ellipses, the strain hardening can be neglected, and the incremental relation between strain and stress is linearly elastic and isotropic, they found that blunting occurs when the maximum cohesive stress σ_0 exceeds Young's modulus by about a factor of two, σ_o/E=2.

The polyampholyte hydrogel showed non-linear large deformation behaviors, exhibiting yielding or strain softening and then strain hardening (**Figure 2**). With the increase of the stretch deformation, the stress concentration at the crack first leaded to yielding around the crack tip due to breakage of weak bonds and then brought about blunting. After the crack was blunted, the polymer chains around the tip were extensively stretched along the tensile direction, in perpendicular to the crack growth direction. Further increase in the deformation led to strain hardening due to limited chain extensibility and then rupture of

the polymer chain, by breaking either of the strong bonds or of the covalent bonds of chains. So the crack started to advance in a triangular shape.

As the balance between the tensile fracture stress and the modulus, and the large stretchability should be important for the occurrence of crack blunting for this non-linear soft material, we summarized the blunting behavior in a σ_f/E - ε_f diagram as shown in **Figure 7**. Here σ_f and ε_f are tensile fracture stress and strain, respectively. We found that when the notched sample was stretched at varied stretching rate, significant blunting was observed when σ_f/E was around 2 or higher. When σ_f/E was between 0.4 and 2, only weak blunting was observed, regardless of the large ε_f. These results suggest that large deformation is not the sufficient condition to cause blunting, and the blunting only occurs when the fracture stress is larger than the modulus.

To confirm whether this conclusion is universal or not, we further studied the tensile and fracture behaviors of the gel at temperature lower than 25°C (**Figure S2**) and at increased ionic strength of the solvent by adding NaCl (**Figure S3**). Reducing of test environmental temperature increases the bond exchange time by suppressing the dissociation of the ionic bonds, and therefore increases the modulus and yielding stress of sample for a fixed deformation rate. On the other side, increase of the ionic strength of the solvent decreases the bond exchange time by suppressing the formation of ion bonds, and therefore decreases the modulus and yielding stress, similar to that of polyelectrolyte complex coacervate.[30] At a decreased temperature, the sample became rigid, showing less significant blunting although the sample still has a large extensibility (data not shown). At an increased ionic strength, the sample became soft, showing more significant blunting(data not shown). These results are also summarized in **Figure 7** and are in

agreement with the previously mentioned conclusions. We found that the PDGI/PAAm hydrogel[14] and the alginate/PAAm hydrogel[13] that showed significant blunting also have σ_f/E values larger than two, as shown in **Figure 7**.

To real at which condition, the blunting vanishes, we further performed the measurement at cooperating conditions of high stretch rate (1.04 s^{-1}) and low temperature (5°C). At this condition, the deformation rate is much faster than the weak bond exchange rate, so the sample became very stiff. As shown in **Figure S4** and **Movie S3**, the sample showed yielding and large deformation, with σ_f/E=0.29 and ε_f =5.6 in tensile test. Furthermore, the sample also showed steady-state crack growth. However, no crack blunting occurred during pure shear test. Also, the stress quickly decreased after it reached a maximum, which is quite different from the previous results for the samples tested at relatively low stretch rate (0.02 s^{-1}) and 25°C. In addition, when the sample was dehydrated from a water content of 52 wt% to 26 wt%, it became stiff and brittle even at room temperature. This sample showed fast breaking from the pre-crack without blunting, as shown in **Figure S5**. These results show that when σ_f/E=0.3 or less, no blunting occurs, regardless a relatively large fracture strain. These results are in consistent with the previous theoretical prediction for linear elastic solid. [19]

Crack advancing angle. In the steady state crack growth stage, the crack advances at a constant angle that decreases with the increase of stretch rate (**Figure 6b**). The stretch rate effects on the shape of the crack tip can be related to the change in the sample modulus and yielding stress that both increases with the stretch rate. According to a finite element analysis for an elastic-plastic solid,[31] the opening angle at the steady state crack

growth θ is proportional to the ratio of the yield stress σ_y to the modulus E. Although this result was obtained for very small value of σ_y/E (~ 0.01) values, we found that this relationship is also true for the present gel that has very large σ_y/E value (~ 0.1). As shown in **Figure 8**, the $\theta E/\sigma_y$ of the polyampholyte gel is a constant, independent of stretch rate over a wide range. This means that θ is proportional to σ_y/E. Furthermore, $\lambda_{c1}E/\sigma_y$ and $\lambda_{c2}E/\sigma_y$ are also independent of the stretch rate (data are not shown), indicating that the critical stretch ratios λ_{c1} and λ_{c2} are proportional to σ_y/E. These results suggest that in the investigated experimental conditions, the initiation and the shape of steady-state crack growth are governed by the ratio of modulus and the yield stress of the gel.

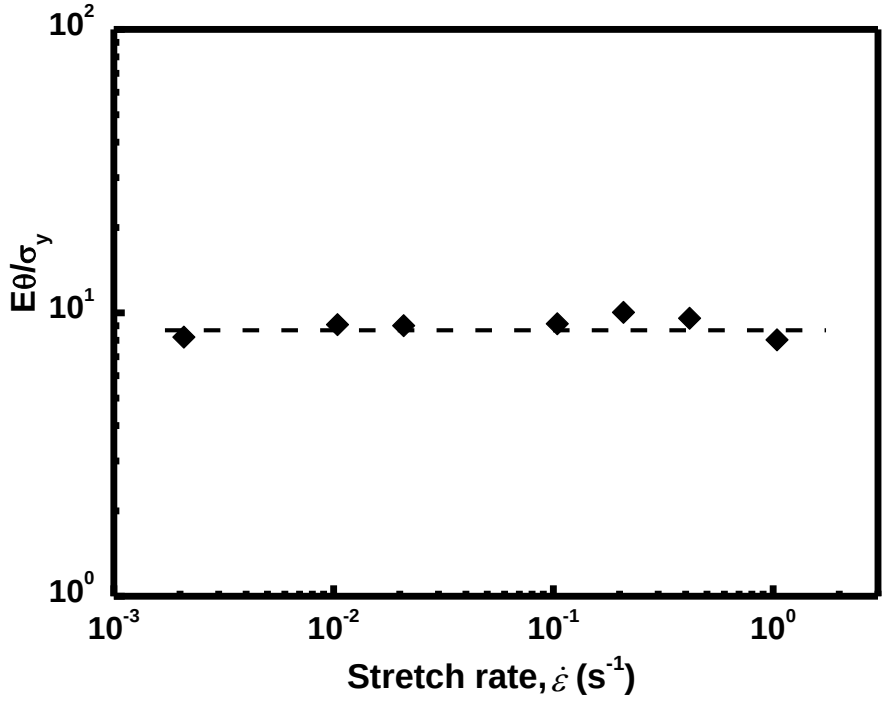

Figure 8. The values of $\theta E/\sigma_y$, as a function of stretch rate. Here θ is the angle of crack during steady state growth, E and σ_y are Young's modulus and yield stress of the sample in tensile deformation, respectively.

Fracture energy. From the results shown in **Figure 2**, we know that this gel has a feature of dual crosslinking structure in the observation time scale. One is reversible and temporary crosslinking by weak ionic bonds, and the other is permanent crosslinking by strong ionic bonds. The strong stretch rate dependence of tensile test results (**Figure 2**) showed that the temporary crosslinker density of weak bonds strongly depends on the observation time. With the increase of the stretch rate, the weak bond crosslinker density increases, giving a strong stretch rate dependence of the modulus E. As the energy required to rupture the sample is mostly use to break these weak bonds, the fracture energy Γ is also strongly depend on the stretch rate (**Figure 3d**). So, we intend to relate the modulus E, which is proportional to the effective crosslinker density at the observation time, to the fracture energy Γ, which is the energy dissipated to break the weak bonds at the same observation time. We plot Γ against E in **Figure 9**, which shows a power law relationship, $\Gamma \sim E^{0.53}$.

We found that the results of Γ and E caused by temperature changes (**Figure S2**) or by ionic strength changes (**Figure S3**) also fall on the same power law relation obtained by the change of the stretch rate, as shown in **Figure 9**. That is, $\Gamma \sim E^{0.53}$ is valid for all of the three sets of samples tuned with different methods.

However, it should be noticed that this correlation between fracture energy and modulus is only hold when the sample was relatively soft, that is, when the deformation rate is less or not very higher than the inverse of the average bond exchange time τ_w of weak bonds. The data obtained at quite high stretch rate (500 mm/min) and low temperature (5°C) or obtained from sample in dehydrated state deviate far from this power law relation. Under these conditions, the deformation rate is much higher than the exchange time of the weak

bonds, the sample became very stiff and the fracture mode changes without showing blunting. The above results indicate when the observation is performed at relatively low deformation rate ($\dot{\varepsilon}\tau_w$ <1), the fracture energy can be related to the small strain modulus of the viscoelastic hydrogel. This is helpful since one can predict the large deformation and fracture behaviors from small deformation.

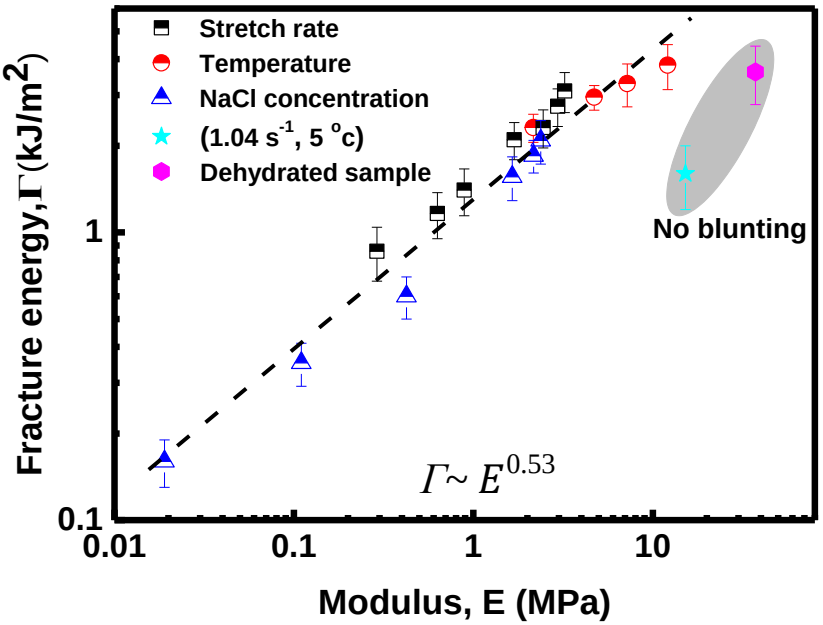

Figure 9. Relationship between the fracture energy Γ and modulus E of the polyampholyte hydrogel. Three sets of data are shown. (1) varied stretch rate (0.002~1.04 s^{-1}), in water, at 25 °C; (2) varied temperature (5 °C, 10 °C, 15 °C, 25 °C), at stretch rate 0.2 s^{-1}, in water; (3) in salt solution (0, 0.05M, 0.1M, 0. 15M, 0.3M, 0.5M), at stretch rate 0.2 s^{-1}, at 25 °C. In all these three measurements, blunting occurred. For comparison, data measured at conditions without blunting are also shown (pentagon: tested at 1.04s^{-1} stretch rate and 5°C; hexagon: tested at dehydrated state with 26 wt% water content, at 0.2 s^{-1} stretch rate and 25°C). Data obtained with blunting all follow a power-law $\Gamma \sim E^{0.53}$, while that without blunting do not fall on the curve.

5. Conclusions

When the stretch rate is not very large ($\dot{\varepsilon}\tau_w$ <1), the polyampholyte physical hydrogel P(NaSS-co-MPTC) exhibits a feature of dually crosslinked network structure, showing yielding, strain softening, and then strain hardening at large deformation. The reduced stress vs time obeys a master curve at various stretch rates, similar to the dually crosslinked PVA system. In the pure shear test, the single-edge notched sample shows crack blunting and butterfly-shaped stress distribution above a critical deformation ratio λ_{c1}. Crack growth occurs above a critical λ_{c2} with a constant advancing angle. The crack only grows under stretching with the same velocity as stretching, showing no spontaneous crack propagation. Because of the dynamic nature of the weak ionic bonds in the polyampholyte hydrogel, the stretch rate greatly influences the crack blunting and advancing angle, thereby influences the fracture energy. The initial modulus E and the fracture stress σ_f of hydrogel both increase with the stretch rate, and their ratio σ_f/E, was found to be a key factor to determine the blunting. On the other hand, the crack advancing angle is linearly proportional to the ratio of yielding stress to modulus σ_y/E. The fracture energy has a power law dependent on the modulus in viscoelastic response region ($\dot{\varepsilon}\tau_w$ <1). These conclusions are universal, hold for the samples tuned not only by stretch rate, but also by temperature and salt solution.

Supporting Information

Figures S1−S5 and Movies S1-S3. This material is available free of charge via the Internet at http://pubs.acs.org.

Acknowledgements

This research was financially supported by a Grant-in-Aid for Scientificfic Research (S) (No. 124225006) from Japan Society for the Promotion of Science (JSPS) and the Grant-in-Aid for JSPS Fellows relating to JSPS Postdoctoral Fellowships for Foreign Researchers (No. P12340) from JSPS.

References

(1) Annabi, N.; Tamayol, A.; Uquillas, J. A.; Akbari, M.; Bertassoni, L. E.; Cha, C.; Camci‐Unal, G.; Dokmeci, M. R.; Peppas, N. A.; Khademhosseini, A. *Adv. Mater.* **2014,** *26* (1), 85-124.

(2) Haque, M. A.; Kurokawa, T.; Gong, J. P. *Polymer* **2012,** *53* (9), 1805-1822.

(3) Okumura, Y.; Ito, K. *Adv. Mater.* **2001,** *13* (7), 485-487.

(4) Gong, J. P. *Soft Matter* **2010,** *6* (12), 2583-2590.

(5) Gao, H.; Wang, N.; Hu, X.; Nan, W.; Han, Y.; Liu, W. *Macromol. Rapid. Comm.* **2013,** *34* (1), 63-68.

(6) Henderson, K. J.; Zhou, T. C.; Otim, K. J.; Shull, K. R. *Macromolecules* **2010,** *43* (14), 6193-6201.

(7) Hunt, J. N.; Feldman, K. E.; Lynd, N. A.; Deek, J.; Campos, L. M.; Spruell, J. M.; Hernandez, B. M.; Kramer, E. J.; Hawker, C. J. *Adv. Mater.* **2011,** *23* (20), 2327-2331.

(8) Gao, H.; Yao, H. *P. Natl. Acad. Sci. USA* **2004,** *101* (21), 7851-7856.

(9) Burattini, S.; Colquhoun, H. M.; Fox, J. D.; Friedmann, D.; Greenland, B. W.; Harris, P. J.; Hayes, W.; Mackay, M. E.; Rowan, S. J. *Chem. Commun.* **2009,** (44), 6717-6719.

(10) Hao, J.; Weiss, R. *Macromolecules* **2011,** *44* (23), 9390-9398.

(11) van de Manakker, F.; van der Pot, M.; Vermonden, T.; van Nostrum, C. F.; Hennink, W. E. *Macromolecules* **2008,** *41* (5), 1766-1773.

(12) Myung, D.; Waters, D.; Wiseman, M.; Duhamel, P. E.; Noolandi, J.; Ta, C. N.; Frank, C. W. *Polym. Advan. Technol.* **2008,** *19* (6), 647-657.

(13) Sun, J. Y.; Zhao, X. H.; Illeperuma, W. R. K.; Chaudhuri, O.; Oh, K. H.; Mooney, D. J.; Vlassak, J. J.; Suo, Z. G. *Nature* **2012,** *489* (7414), 133-136.

(14) Haque, M. A.; Kurokawa, T.; Kamita, G.; Gong, J. P. *Macromolecules* **2011,** *44* (22), 8916-8924.

(15) Sun, T. L.; Kurokawa, T.; Kuroda, S.; Ihsan, A. B.; Akasaki, T.; Sato, K.; Haque, M. A.; Nakajima, T.; Gong, J. P. *Nat. Mater.* **2013,** *12* (10), 932-937.

(16) Nakajima, T.; Kurokawa, T.; Furukawa, H.; Yu, Q. M.; Tanaka, Y.; Osada, Y.; Gong, J. P. *Chinese J. Polym. Sci.* **2009,** *27* (1), 1-9.

(17) Taylor, D.; O'Mara, N.; Ryan, E.; Takaza, M.; Simms, C. *J.Mech. Behav. Biomed. Mater.* **2012,** *6*, 139-147.

(18) Mayumi, K.; Marcellan, A.; Ducouret, G.; Creton, C.; Narita, T. *Acs Macro. Lett.* **2013,** *2* (12), 1065-1068.

(19) Hui, C.-Y.; Jagota, A.; Bennison, S.; Londono, J. *Proc. R. Soc. Lond. A* **2003,** *459* (2034), 1489-1516.

(20) Ihsan, A. B.; Sun, T. L.; Kuroda, S.; Haque, M. A.; Kurokawa, T.; Nakajima, T.; Gong, J. P. *J. Mater. Chem. B* **2013,** *1* (36), 4555-4562.

(21) Rivlin, R.; Thomas, A. G. *J. Polym. Sci.* **1953,** *10* (3), 291-318.

(22) Kim, B. S.; Chen, L.; Gong, J. P.; Osada, Y. *Korea Polym. J.* **2000,** *8* (3), 116-119.

(23) Bloss, F. D., *An introduction to the methods of optical crystallography*. Holt Rinehart and Winston: 1961.

(24) Wu, Z. L.; Sawada, D.; Kurokawa, T.; Kakugo, A.; Yang, W.; Furukawa, H.; Gong, J. P. *Macromolecules* **2011,** *44* (9), 3542-3547.

(25) Baumberger, T.; Caroli, C.; Martina, D. *Nat. Mater.* **2006,** *5* (7), 552-555.

(26) Bucknall, C.; Paul, D. *Polymer* **2009,** *50* (23), 5539-5548.

(27) Kobayashi, A.; Chan, C. *Exp. Mech.* **1976,** *16* (5), 176-181.

(28) Rahul-Kumar, P.; Jagota, A.; Bennison, S.; Saigal, S.; Muralidhar, S. *Acta Mater.* **1999,** *47* (15), 4161-4169.

(29) Jagota, A.; Bennison, S.; Smith, C. *Int. J. Fract.* **2000,** *104* (2), 105-130.

(30) Spruijt, E.; Cohen Stuart, M. A.; van der Gucht, J. *Macromolecules* **2013,** *46* (4), 1633-1641.

(31) Tvergaard, V.; Hutchinson, J. W. *J.Mech. Phys.Solids* **1992,** *40* (6), 1377-1397.

For Table of Contents Use Only

Crack Blunting and Advancing Behaviors of Tough and Self-healing Polyampholyte Hydrogel

Feng Luo[1†], Tao Lin Sun[1†], Tasuku Nakajima[1], Takayuki Kurokawa[1], Yu Zhao[2], Abu Bin Ihsan[1], Hong Lei Guo[2], Xu Feng Li[2] and Jian Ping Gong[1*]

[1]*Faculty of Advanced Life Science, Hokkaido University, Sapporo 060-0810, Japan*

[2]*Graduate School of Life Science, Hokkaido University, Sapporo 060-0810, Japan*

*Corresponding author: gong@mail.sci.hokudai.ac.jp

[†]These authors contributed equally to this work.